ACS OMEGA

http://pubs.acs.org/journal/acsodf

Article

Physical and Chemical Properties of Coal Gasification Fine Slag and Its Carbon Products by Hydrophobic−Hydrophilic Separation

Zhonghua Xue, Lianping Dong,* Xiaoting Fan, Zhenyang Ren, Xiaodong Liu, Panpan Fan, Minqiang Fan, Weiren Bao, and Jiancheng Wang

Cite This: *ACS Omega* 2022, 7, 16484−16493

Read Online

ACCESS | Metrics & More | Article Recommendations

ABSTRACT: Coal gasification fine slag is a kind of solid waste with low resource utilization rate. The complex embedding of residual carbon and inorganic minerals (ash materials) is the main reason restricting the efficient resource separation and utilization of residual carbon or ash materials. Hydrophobic−hydrophilic separation (HHS) is a separation technology in which mineral particles with different surface hydrophobicity values are enriched in the water phase and oil phase under the action of mechanical stirring. The water on the surface of hydrophobic particles is replaced by the oil phase to form flocs, which are enriched in the hydrophobic liquid phase, while hydrophilic particles are dispersed into the aqueous phase. In this study, the HHS process was used to separate the carbon/ash from the fine gasification slag produced by a Shenning gasifier, Texaco gasifier, and GSP gasifier of Ningxia Coal Industry Co., Ltd. The physicochemical properties of the original sample and the residual carbon products obtained by hydrophobic−hydrophilic separation were analyzed. The results show that HHS can separate the carbon/ash in the three kinds of fine slag to varying degrees. The carbon element is enriched into the hydrophobic phase to form the concentrates, while the silicon element, oxygen element, and metal element enter the tailings. The spherical ash with different particle sizes distributed on the surface of residual carbon and the gap of the matrix is basically removed, while the ash in the carbon−ash melt is difficult to remove. The ash contents of the concentrate and tailings of fine slag of the Shenning gasifier are 22.58 and 96.28%, respectively, which reach the best ash index compared with that of the other two gasifiers. From the change of mineral surface properties after HHS, the distribution of oxygen-containing groups, benzene rings, Si−O, and clay minerals or carbonate minerals in the three kinds of fine slag residual carbon products is basically similar. Compared with the other two gasifier products, the GSP gasifier concentrate has a larger specific surface area and less ash material, more amorphous carbon structures (less graphitic), and more active sites, resulting in a stronger combustion activity.

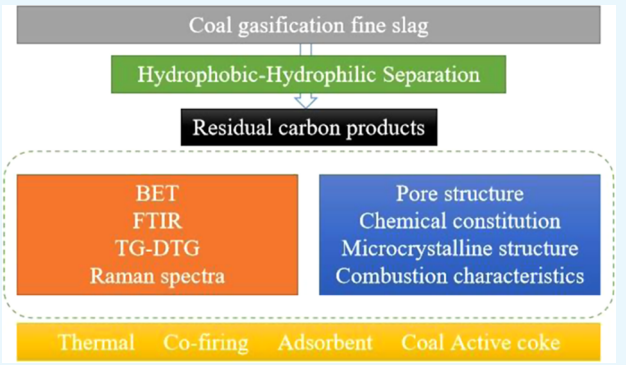

1. INTRODUCTION

Coal plays an important role in the energy production and chemical fields of China, the world's largest coal producer and consumer.[1] The modern coal chemical industry is an effective way to transform coal from single fuel to diversified utilization of coal. Coal gasification is the preprocess of coal-derived chemicals, coal-based synthetic natural gas, liquid fuels made from coal, integrated gasification combined cycle (IGCC), and other processes. It is expected that by the end of the 14th "five-year plan", the amount of transformed coal will reach about 160 million tons.[2,3]

In the process of coal gasification, coarse and fine slags are produced. The coarse slag is directly discharged at the bottom of the gasifier; the fine slag enters the riser in the form of fly ash and is discharged together with the flue gas and generated through the slag discharge process. The incomplete reaction of carbon in the coal gasification process results in a certain amount of residual carbon in the gasification slag.[4]

Present research into the utilization of coal gasification slag focuses mainly on two aspects. The first is the use of slag to prepare construction materials. According to GB/T 1596-2017, the loss on ignition of grade I fly ash required for mixing cement concrete and mortar and in the admixture used as an active mixture in cement production is not more than 5%.[5] The second focus is on recycling, blending, and improving the quality of residual carbon. Circulating and mixed combustion are

Received: January 24, 2022
Accepted: April 26, 2022
Published: May 4, 2022

https://doi.org/10.1021/acsomega.2c00484
ACS Omega 2022, 7, 16484−16493

conducive to reducing loss on ignition and facilitate the subsequent utilization of coal gasification slag as a building material. The product obtained after upgrading carbon residue is mainly used to prepare activated carbon. It is also used as an adsorbent because it contains a large specific surface area and pore volume and can effectively adsorb iodine, methylene blue, and the heavy metal Cr^{3+}.[6,7] The separation of residual charcoal and inorganic minerals is the essential step toward increasing its utilization.[8,9]

Various recent research studies have examined the separation and enrichment of residual carbon in gasification slags, including using gravity concentration and froth flotation. Gravity concentration relies on the density difference between the residual carbon and ash material components.[10−12] Ren et al.[13] used a water hydrocyclone to classify gasification fine slags, separated the high-carbon products on the overflow screen to prepare the gasification slag-based active coke, and evaluated its desulfurization and denitrification performance. Their test verified the feasibility of gravity separation of gasification slags and the use of high-carbon products as active coke raw materials. After relieving the pressure of the gasification slag treatment, its resource utilization is further realized. However, it does not involve the resource utilization of fine-grain grade (−0.074 mm). Froth flotation is a commonly used fine-grain mining method. Wu[11] conducted a series of direct and reverse flotation tests on residual carbon and found that the effects of separating residual carbon from gasification slag in reverse flotation tests were better than those in direct flotation tests, and the ash content in high-ash products was under 90%. For better improvement of flotation-based separation effects, multiple methods were introduced into the research, such as flotation column-based flotation, multistep flotation, pregrinding treatment, carrier flotation, ultrasonic pretreatment of the pulp, and the ultrasonic treatment and reagent method.[14−22] Zhang et al.[23] systematically studied the water-holding capacity, chemical structure, microstructure, and pore characteristics of gasification slag and its separation products, to realize the efficient dehydration of coal gasification slag and the comprehensive utilization of coal/ash separation.

The characteristics of high porosity, large specific surface area, significant surface oxidation, poor hydrophobicity, and flocculant residue in the dehydration process lead to high consumption of flotation reagent and poor economy performance. The steps of reducing reagent consumption by technical improvement are quite complex.[14]

Hydrophobic−hydrophilic separation (HHS),[24] a phenomenon driven by the principle of dewatering by displacement (DBD),[25] enables the efficient separation of hydrophobic and hydrophilic particles (Figure 1). The DBD principle states that hydrophobic fluid spontaneously removes water on the hydrophobic surface and spreads it out into the hydrophobic oil reservoir. Dewatering in HHS is achieved by the displacement of the hydrophobic particle surface by shear dispersion. Hydrophobic particles form floccules that enrich the hydrophobic liquid phase, while hydrophilic particles disperse into the liquid phase. The separation of hydrophobic and hydrophilic particles is thus achieved via phase separation. After recycling hydrophobic products with a hydrophobic liquid, its water content is very low, which eliminates the need for subsequent thermal drying and greatly reduces the recovery cost. This makes HHS an advanced technology for integrating separation and dehydration. Xue et al.[26] extended HHS to the carbon/ash separation of coal gasification fine slag and studied the influence

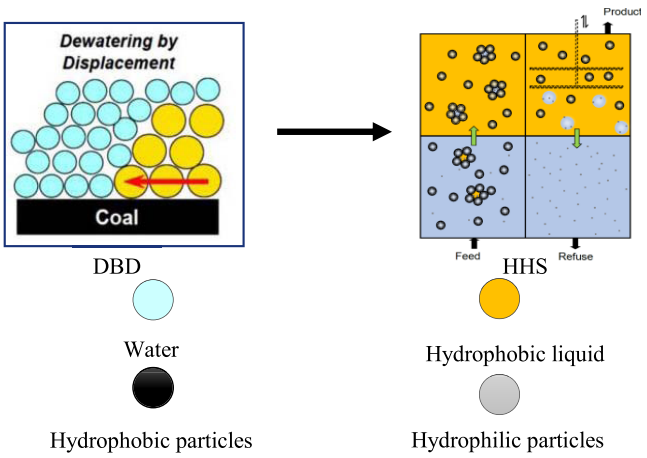

Figure 1. Illustration of dewatering by displacement (DBD) and hydrophobic−hydrophilic separation (HHS).

of the energy input (mixing strength and mixing time) and hydrophobic liquid dosage on the separation effect. They analyzed the separation mechanism of coal gasification fine slag using a ζ-potential analysis, a contact-angle analysis, an X-ray photoelectron spectroscopy (XPS) analysis, and extended DLVO theory. This provided a theoretical basis for further strengthening the carbon/ash separation mechanism. They compared the flotation results with HHS results and found that HHS not only has a simple process but also has a low ash content in the concentrate and a high ash content in the tailings when the concentrate yield is similar, which fully shows that HHS has obvious advantages over flotation.

This study used HHS to study the physical and chemical properties of three coal gasification fine slags and their products. The elemental composition and distribution, chemical structure, micromorphology, pore characteristics, microcrystal structure, and combustion characteristics of coal gasification fine slag and its residual carbon products were systematically studied using ultimate analysis, SEM-EDS, BET, XRF, FTIR, Raman spectra, and thermogravimetric analysis. The aim is to provide a theoretical basis and technical support for reusing HHS.

2. EXPERIMENTAL SECTION

2.1. Particle Size Composition. In this study, the three kinds of coal gasification fine slag were wet-screened to analyze the change of particle size composition.

According to Table 1, the total ash content varies in the order SNL_Y (78.39%) > DSG_Y (77.20%) > GSP_Y (65.10%). The cumulative ash scores of 0.074−0 mm for SNL_Y and DSG_Y exceed 82% and those of 0.074−0 mm for GSP_Y reaches 66.04%. The contents of the three fine-grain grades (0.074−0 mm) vary in the order DSG_Y (78.04%) > GSP_Y (67.12%) > SNL_Y (65.21%). The residual carbon is enriched in the particle size range of 0.074−0 mm, which is difficult to separate by flotation. SNL_Y, DSG_Y, and GSP_Y are more suitable for achieving the efficient selection of fine particle minerals by the HHS process.

2.2. HHS. The HHS test was performed in an XFD flotation machine with a 1 L flotation tank. Figure 2 shows the 50 g sample placed in the flotation tank.[26] After adding 1 L of water, the mixing impeller was opened for 5 min (2250 rpm) to fully moisten the sample, and *n*-heptane ($m_{n\text{-heptane}}/m_{sample}$ = 2:5) was added for 5 min. The slurry was then transferred to a 2 L split drain for 5 min to let the particles settle in the water phase and to release the oil phase to another beaker as the concentrate. The

https://doi.org/10.1021/acsomega.2c00484
ACS Omega 2022, 7, 16484−16493

Table 1. Particle Size Composition in the Sample[a]

	SNL_Y		DSG_Y		GSP_Y	
size (mm)	yield (%)	ash content (%)	yield (%)	ash content (%)	yield (%)	ash content (%)
0.5−0.25	10.99	87.57	5.87	33.33	12.40	62.83
0.25−0.125	10.98	64.77	8.65	42.09	9.43	73.53
0.125−0.074	12.82	61.65	7.44	64.74	11.05	54.73
0.074−0.045	11.47	72.16	10.74	81.75	13.76	49.70
0.045−0	53.74	84.61	67.30	86.18	53.36	70.25
total	100.00	78.39	100.00	77.20	100.00	65.10

[a]Shenning coal gasification fine slag − SNL_Y, Texas coal gasification fine slag − DSG_Y, GSP coal gasification fine slag − GSP_Y, the concentrate of Shenning coal gasification fine slag − SNL_C, Texas coal gasification fine slag − DSG_C, GSP coal gasification fine slag − GSP_C.

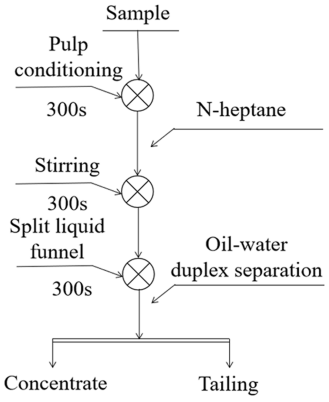

Figure 2. Schematic experimental process.

concentrates and tailings were filtered and dried in a vacuum oven (120 °C). The concentrate yield, concentrate ash, ash in tailings, combustible recovery, noncombustible recovery, and separation efficiency were calculated as follows.

The combustible recovery ε (%) reflects the degree of combustible carbon recovery of refined products relative to the initial material.

$$\varepsilon = \frac{\gamma_j(100 - A_i)}{100 - A_y} \times 100\% \quad (1)$$

where γ_j denotes the concentrate yield and A_i is the raw material ash (%). The noncombustible recovery ε (%) reflects the recovery of noncombustible ash material compared with

$$\varepsilon = \frac{\gamma_j A_i}{A_y} \times 100\% \quad (2)$$

The separation efficiency E (%) is the difference between combustible recovery and noncombustible recovery, which comprehensively reflects the separation effect of coal-gasified fine slag

$$E = \varepsilon - \varepsilon \quad (3)$$

2.3. Experimental Methods. An Elemantar:Vario EL cube was used to determine the ultimate analysis of the samples. A VBR-6000 was used to determine the bomb calorific value.

The surface pore structure of the residual charcoal and ash material particles was analyzed using an ASAP 2460 2.01 BET nitrogen adsorption-specific surface instrument. The measurement conditions were as follows: maintaining the heating rate at 10.0 °C/min, the temperature at 200.0 °C, and the pressure at 100 mmHg for 600 min.

The surface morphology and elemental composition of the samples were analyzed using a scanning electron microscope energy spectrometer (SEM-EDS, Rigaku MiniFlex 600).

A Thermo Fischer ESCALAB 250Xi was used for X-ray photoelectron spectroscopy (XPS) measurements, which utilizes the element difference in electron binding energies and determines the elements present in the samples based on photoelectron absorption peaks.

After removing carbon from each sample, XRF analysis was performed using an ARL PERFORM'X, where decarbonization was performed using the slow ash method to heat the sample at the maver furnace.

A Thermo Scientific Nicolet iS5 Fourier transform infrared spectrometer was used for the functional analysis of the gasification slags before and after reaction with the collectors. In each measurement, a 1 mg solid sample was mixed with 100 mg of potassium bromide, ground to −0.2 μm, and pressed into tablets for 60 s at 10 MPa. The measurement results were analyzed using the OMNIC spectral analysis software package.

Raman spectra reported here were recorded under natural air conditions and at room temperature using a Horiba Scientific LabRAM HR Evolution spectrometer with a back-scattered configuration and equipped with a Nd:YAG laser at 512 nm as its light source for Raman spectroscopy. The instrument is not a microscope. A laser power of 2 mW was selected. The spectral resolution was 2 cm^{-1}.

The combustion reactivity of the sample was tested using a thermogravimetric analyzer (NETZSCH STA 449F3). The sample was heated from 23 to 900 °C at a rate of 5 °C/min and with a total air flow rate of 100 mL/min. The combustion atmosphere selected was a 21% O_2/79% N_2 mixture to simulate the air atmosphere.

Table 2. Results of HHS

item	concentrate yield (%)	concentrate ash content (%)	tailing ash content (%)	combustible recovery (%)	noncombustible recovery (%)	separation efficiency (%)
SNL_Y	22.58	20.60	96.28	84.38	5.74	78.64
DSG_Y	37.33	22.98	86.90	58.80	11.36	47.44
GSP_Y	21.34	31.11	83.71	68.56	10.34	58.24

https://doi.org/10.1021/acsomega.2c00484
ACS Omega 2022, 7, 16484−16493

3. RESULTS AND DISCUSSION

3.1. Experimental Results of HHS. The purpose of carbon/ash separation is to reduce the concentrate ash content and increase the ash content of tailings. Carbon/ash separation outcomes are listed in Table 2 for the three samples following different sorting processes. The concentrate ash scores of SNL_Y and GSP_Y are below 23%, and the highest SNL_Y tailing ash score is 96.28%. This can serve as a filling in bulk building materials and coal mines or as a source of activated powder in construction.[27] The maximum concentrate yield of GSP_Y is 31.11%, and the maximum combustible recovery and separation efficiencies of SNL_Y are 84.38 and 78.64%, respectively. The results show that carbon/ash separation in gasification fine slag can be achieved by HHS. Based on the concentrate ash, tailing ash, and combustible recovery, SNL_Y displays optimal carbon/ash separation, followed by GSP_Y, while DSG_Y gives the worst result.

3.2. Basic Properties of Coal Gasification Fine Slag and Residual Carbon Products. *3.2.1. Basic Properties.* The results of the ultimate analysis and bomb calorific value tests are listed in Table 3. After HHS, the carbon content of SNL_Y increased from 18.74 to 72.29%, that of DSG_Y increased from 18.36 to 58.16%, and that of GSP_Y increased from 33.81 to 74.79%. Compared with the original sample, the bomb calorific values for the three coal gasification fine slags were increased to above 22.40 MJ/kg, with SNL_Y showing the greatest improvement. The concentrate products can be used as thermal coal, for thermal combustion, for regasification, etc.[28]

Table 3. Ultimate Analysis and Bomb Calorific Values of the Sample and Its Products

	ultimate analysis (%)					bomb calorific values (MJ/kg)
item	C_d	H_d	O_d	N_d	$S_{t,d}$	$Q_{b,ad}$
SNL_Y	19.18	0.18	0.41	0.12	0.31	5.91
SNL_C	72.29	1.73	1.84	0.30	0.73	26.50
DSG_Y	18.36	0.41	0.09	0.13	0.25	5.48
DSGc	58.16	1.75	6.77	0.26	0.69	22.47
GSP_Y	33.81	0.80	4.20	0.34	0.65	11.41
GSPc	74.79	1.40	5.52	0.51	0.91	26.66

The pore structure parameters of the gasification fine slag and its residual carbon products are shown in Table 4, and the pore diameter distribution is plotted in Figure 3. Coal gasification fine slag is rich in medium pores and micropores, and the number of holes within each aperture range varies greatly. Among the three types of coal gasification fine slag, the particle surface pore structure of DSG_Y is the most developed, showing the largest specific surface area and pore volume. This phenomenon has a significant effect on the HHS of coal gasification fine slag. The developed pore structure absorbs a large amount of water and hydrophobic liquid. This not only consumes many agents and reduces the sorting effect but also makes the removal of oil and water challenging. After HHS, DSG_C has the most developed pores and abundant micropores, with a larger specific surface area and pore volume than those of the other products. This raw material is therefore well-suited for preparing[13] active coke and activated carbon adsorption materials.

Table 4. Nitrogen Adsorption Test Results for the Sample and Its Products

samples	BET surface area (m^2/g)	total pore volume (cm^3/g)	*t*-plot micropore volume (cm^3/g)	average pore diameter (nm)
SNL_Y	99.14	0.1233	0.0136	4.98
SNL_C	195.49	0.2808	0.0112	5.75
DSG_Y	215.48	0.3047	0.0266	5.65
DSGc	359.22	0.6885	0.0195	6.95
GSP_Y	186.02	0.2060	0.0247	4.43
GSPc	279.65	0.3736	0.0145	5.34

3.2.2. Microscopic Morphology and Element Distribution. An SEM-EDS analysis of the coal gasification fine slag and residual carbon products was conducted. The main components of the irregular block and porous surface are residual carbon particles[29] (Figure 4 and Table 5). The carbon content of the original SNL_C sample (point b on Figure 4) and of GSP_C (point f) exceeds 90%. The smooth ball consists mainly of ash particles and has a similar element composition, mainly composed of C, O, Al, and Si (respectively, points a, c, and e in Figure 4). All three samples feature a carbon/ash distribution of residual carbon surface attachment and carbon−ash melting and the residual carbon body pores in SNL_Y and GSP_Y. In the concentrate, the sizes of the two forms of the carbon/ash distribution are essentially removed and presented as three forms of layer floc, porous mesh, and carbon−ash melting. The carbon/ash embedded in the molten state is difficult to be separated by HHS. Based on the selectivity of molten substances to different phases, part of the carbon/ash melt enters the concentrate, and the ash contained in it leads to the ash content of the concentrate being 20−40%. At 20 000 times the diameter, the GSP_C has the densest space, consistent with the hole structure parameters given in Table 4.

Table 5 and Figure 5 show the relative element compositions of the three coal gasification fine slags and residual carbon products, C 1s, O 1s, Si 2p, and Al 2p. They indicate that HHS effectively removes ash material containing O, Si, and Al, consistent with the SEM-EDS results.

3.2.3. XRF Analysis. Table 6 reports the XRF analysis results for the three kinds of coal-gasified fine slags and their residual carbon products. The sample ash is mainly composed of SiO_2, Al_2O_3, Fe_2O_3, and CaO, while the SiO_2 content is 44−54% and Al_2O_3 accounts for more than 15%. The Al_2O_3 contents of DSG_Y and DSG_C are more than 20%, indicating that they contain a large amount of clay minerals. When the sample and concentrate have an equivalent ash content, there is relatively little Si, Al, Fe, and Ca, which achieve the purpose of separation. This is consistent with the distribution of the prototype and its carbon/ash product, as determined by SEM-EDS. After HHS, many spheroids were detached and enriched the tailings, facilitating the subsequent reuse of ash material components.

3.3. Chemical Properties of the Carbon Products. *3.3.1. Chemical Constitution.* The results of the infrared spectroscopic analysis done on the concentrates of the three kinds of gasification slags are given in Figure 6. The functional groups, listed in Table 7, are associated with the following bands: C═O (1250−1000 cm^{-1}), −COOH (1640−1540 cm^{-1}), and −OH and N−H (3700−3200 cm^{-1}). These indicate that the large oxygen-containing groups on the surface of the gasification slag easily form intermolecular hydrogen bonds with H_2O molecules when ionized in water, which in turn makes it difficult to perform froth flotation. The weak absorption peak at 1500 cm^{-1} represents the existence of the benzene ring in the coal gasification fine slag. In addition, the bands at 1100−1000 and 600−400 cm^{-1} correspond to the characteristic peaks of Si−O−

https://doi.org/10.1021/acsomega.2c00484
ACS Omega 2022, 7, 16484−16493

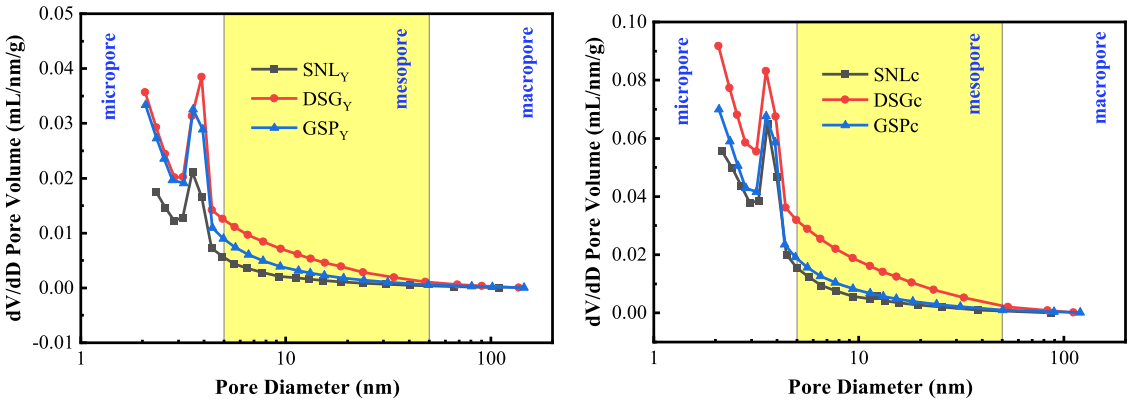

Figure 3. Pore structure of the sample and its products.

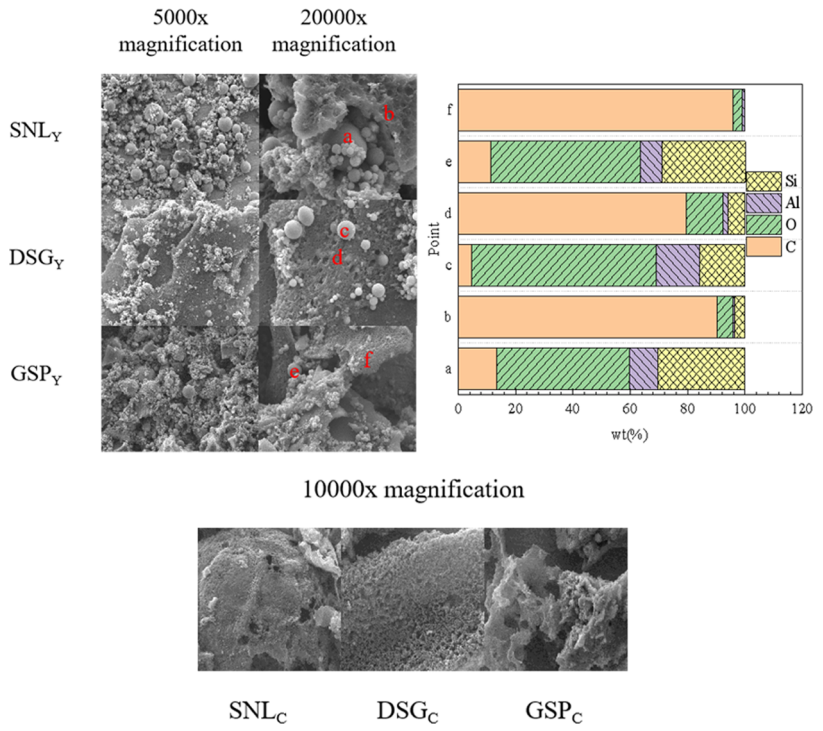

Figure 4. SEM-EDS analysis of the sample and its products.

Table 5. Surface Element Composition (%) of the Sample and Its Products (XPS)

	C 1s	O 1s	Si 2p	Al 2p
SNL$_Y$	56.77	31.32	8.85	3.06
SNL$_C$	84.57	11.42	2.56	1.42
DSG$_Y$	73.75	20.11	1.98	4.16
DSGc	85.84	11.07	1.9	1.2
GSP$_Y$	69.12	23.24	4.71	2.92
GSPc	84.9	11.48	2.17	1.45

Si and the fingerprint region of clay minerals or carbonate minerals, representing the carbon product containing some ash material.

3.3.2. Microcrystalline Structure. The Raman spectra feature two distinct peaks, namely the "defect" (D) and "graphite" (G) peaks. The concentrate described in this paper is a complex carbon material, displaying 10 Raman spectral bands between 800 and 1800 cm^{-1}.[30,31]

The Raman peak positions (Figure 7) and their attributions are listed in Table 8, together with the corresponding fitting parameters. The G-peak full width at half maximum (FWHM-G) varies inversely with the degree of aromatization of the sample. The lower the value of the ratio AD/AG, the nearer is the structure to that of graphite. The ratio (AGR + AVL + AVR)/AD determines the relative proportions of 3−5 aromatic rings and the large ring structure of six aromatic rings.[31] The ignition temperature of the sample increased with aromatization and was jointly affected by the content ratios of small, medium, and large ring structures and pore structures. A comparison of the Raman spectral parameters for each carbon product (Table 9) reveals a variation in the ratio size of FWHM-G for the three samples in the order SNL$_C$ > GSP$_C$ > DSG$_C$, which indicates that there is a higher aromatic degree of DSG$_C$. The ordering of the AD/AG ratio is GSP$_C$ > DSG$_C$ > SNL$_C$, indicating SNL$_C$ is closer to the graphite structure and that GSP$_C$ contains a higher proportion of amorphous carbon. The ordering of the (AG$_R$ + AV$_L$ + AV$_R$)/AD ratio is SNL$_C$ > DSG$_C$ > GSP$_C$. This indicates

https://doi.org/10.1021/acsomega.2c00484
ACS Omega 2022, 7, 16484−16493

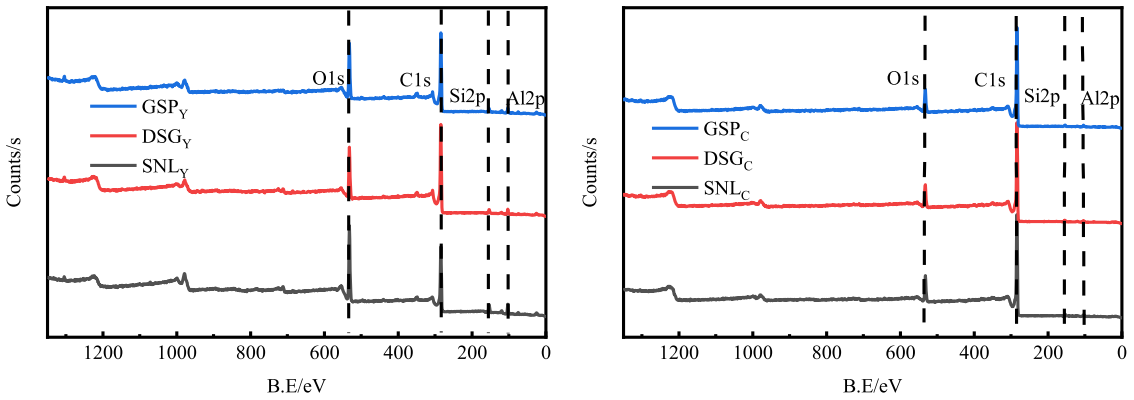

Figure 5. Element composition on the sample surface (XPS).

Table 6. XRF Results of the Sample and Its Products

item	SiO_2	Al_2O_3	Fe_2O_3	CaO	MgO	SO_3	K_2O	Na_2O	TiO_2	P_2O_5	total
SNL_Y	53.78	15.02	10.08	9.01	3.11	2.79	1.94	1.87	1.14	0.42	99.16
SNL_C	50.49	15.36	11.96	9.17	3.17	2.68	2.16	1.63	1.28	1.21	99.11
DSG_Y	45.76	20.18	9.44	10.05	3.98	0.84	1.98	4.41	0.96	0.23	97.83
DSG_C	44.05	20.03	9.20	11.26	4.50	2.33	2.18	3.67	1.20	0.47	98.89
GSP_Y	50.70	19.01	8.49	10.87	3.23	1.49	1.72	1.65	0.91	0.32	98.39
GSP_C	45.68	15.81	11.97	12.99	4.02	2.73	1.83	1.39	1.24	1.36	99.02

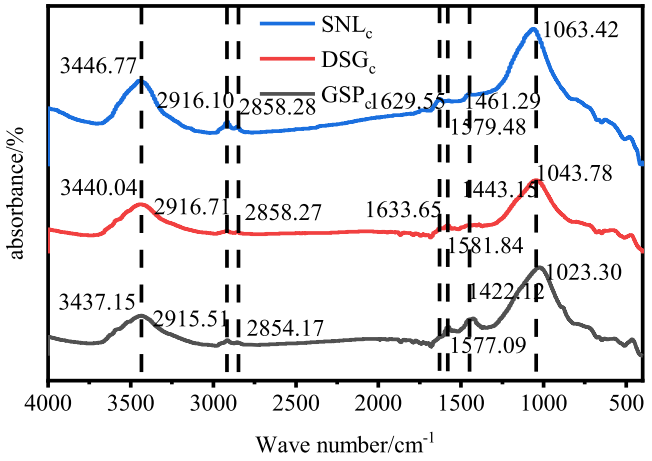

Figure 6. FTIR spectra of the residual carbon products.

Table 7. Functional Group Types and Their Corresponding Absorption Peak Range

absorption peak range (cm^{-1})	functional group types
3750−3000	characteristic peaks of −OH and N−H
3100−2750	aliphatic vibration region of C−H
3550−3450	intermolecular hydrogen bond−dimolecule association
3500−3200	intermolecular hydrogen bond−multimolecular association
2954.44, 2922.56, and 2854.25	telescopic vibration of C−H in saturated alkane hydrogen
1640−1540	telescopic vibration of C═O
1500	the skeleton vibration of the benzene class
1470−1450	telescopic vibration of C−H in $-CH(CH_3)_2$
1250−1000	alcohol-type C−O telescopic vibration absorption peak
1100−1000	telescopic vibration of Si−O−Si
600−400	clay minerals or carbonate minerals

that the large aromatic ring system is more for GSP_C. Taken together, these results provide a theoretical basis for the study of the combustion characteristics of residual carbon products.

3.3.3. Combustion Characteristics. The thermal weight (TG-DTG) joint definition method was used to determine the ignition temperature, the maximum combustion rate, the peak temperature, the exhaust temperature, and the comprehensive combustion characteristic index to evaluate the combustion performance of the fuel.[32−34]

The ignition temperature (t_i) is determined by first plotting the tangent at the midpoint of the TG curve (point B in Figure 8). Then, the intersection of this line with the maximum level of the curve, defined as point C, determines the fire temperature t_i.

Burnout temperature (t_h) is the corresponding temperature when the coal sample conversion rate was 99%. Maximum combustion rate (W_{max}) is the peak on the DTG curve. The average combustion rate W_{mean} (%/min) was calculated as

$$W_{mean} = \beta \cdot \frac{\alpha_i - \alpha_h}{t_h - t_i} \quad (4)$$

where β is the heating rate (°C/min), α_i is the mass fraction of the test sample fire (%), and α_h is the mass fraction of the sample burned out (%). The integrated combustion characteristic index S is given by

$$S = \frac{W_{max} - W_{mean}}{t_i^2 \times t_h} \quad (5)$$

where W_{max} is the maximum weight loss rate (%/min), t_i is the ignition temperature (°C), and t_h is the burnout temperature (°C).

Figure 8 shows three types of concentrate combustion that occur predominantly at three stages. First is the water drying phase, which mainly features carbon water adsorption, causing carbon product loss. According to BET and FT-IR spectral analyses, the adsorption of water molecules occurs mainly because it is favored by the carbon product pore structure. Also, the surface has more hydrophilic oxygen functional groups and

https://doi.org/10.1021/acsomega.2c00484
ACS Omega 2022, 7, 16484−16493

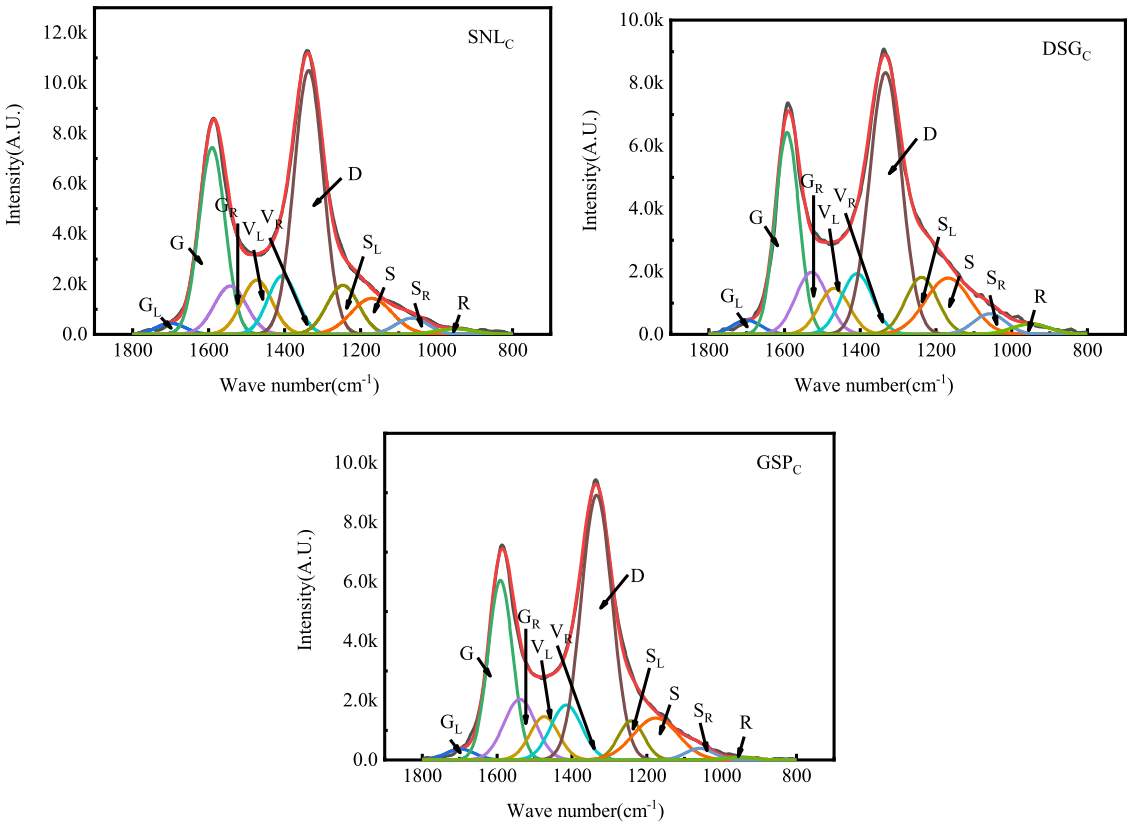

Figure 7. Raman spectra of the residual carbon products.

Table 8. Summary of Raman Peak/Band Assignments (1800−800 cm^{-1})

band name	band position (cm^{-1})	description	band type
G_L	1700	carbonyl group C═O	sp2
G	1590	aromatic ring quadrant breathing, alkene C═C	sp2
G_R	1540	aromatics with 3−5 rings, amorphous carbon structures	sp2
V_L	1465	methylene or methyl, semicircle breathing of aromatic rings, amorphous carbon structures	sp2, sp3
V_R	1415	methyl group; semicircle breathing of aromatic rings; amorphous carbon structures	sp2, sp3
D	1350	D band on highly ordered carbonaceous materials, C−C	sp2
S_L	1230	between aromatic rings and aromatics with no less than six rings aryl−alkyl ether; para-aromatics	sp2, sp3
S	1185	$C_{aromatic}$−C_{alkyl}; aromatic (aliphatic) ethers, C−C on hydroaromatic rings, hexagonal diamond carbon sp^3, C−H on aromatic rings	sp2, sp3
S_R	1060	C−H on aromatic rings, benzene (ortho-di-substituted) ring	sp2
R	960−800	C−C on alkanes and cyclic alkanes; C−H on aromatic rings	sp2, sp3

Table 9. Raman Spectroscopic Parameters of the Residual Carbon Products ("A" Represent "Area")

item	FWHM-G	AD/AG	$(AG_R + AV_L + AV_R)/AD$
SNLc	80.99	1.58	0.64
DSGc	73.90	1.74	0.63
GSPc	76.85	1.87	0.59

provides hydrophilic adsorption sites for water molecules. The second stage is the volatile analysis of the combustion stage. After the first peak of the DTG curve, the rate of weight loss decreases gradually. When the volatile analysis of the combustion has proceeded to some extent, the fixed carbon begins to burn. This is the third stage of fixed carbon combustion, which proceeds until the fixed carbon is fully combusted.

The characteristic parameters of the combustion curves are listed in Table 10. The ignition-point temperature does not vary significantly. However, the burnout temperatures of the SNL_C and the DSG_C are, respectively, 100.09 and 80.02 °C higher than those of the GSP_C. The DTG curve shows the weight peak during the burning phase being narrower and higher for GSP_C than for SNL_C with DSG_C. This indicates that the residual carbon combustion process in GSP_C is more rapid and intense. This results mainly from the residual carbon in GSP_C, which has a large specific surface area with less gray matter, to accelerate the diffusion capacity of the air. More amorphous (and less graphitic) carbon structures and higher active sites strengthen their combustion activity. The residual carbon in GSP_C burns fastest. The residual carbon in SNL_C has a higher proportion of 3−5 aromatic rings, but it has the smallest specific surface area, resulting in the slowest air diffusion capacity and the minimum average combustion rate. The weight peak of DSG_C is narrower and higher than that of SNL_C and has the largest specific surface area (Table 4). However, it has more ash material (inorganic minerals), which affects its combustion properties. In terms of the comprehensive combustion characteristic indices, the samples are ranked as GSPC > DSG_C > SNL_C.

https://doi.org/10.1021/acsomega.2c00484
ACS Omega 2022, 7, 16484−16493

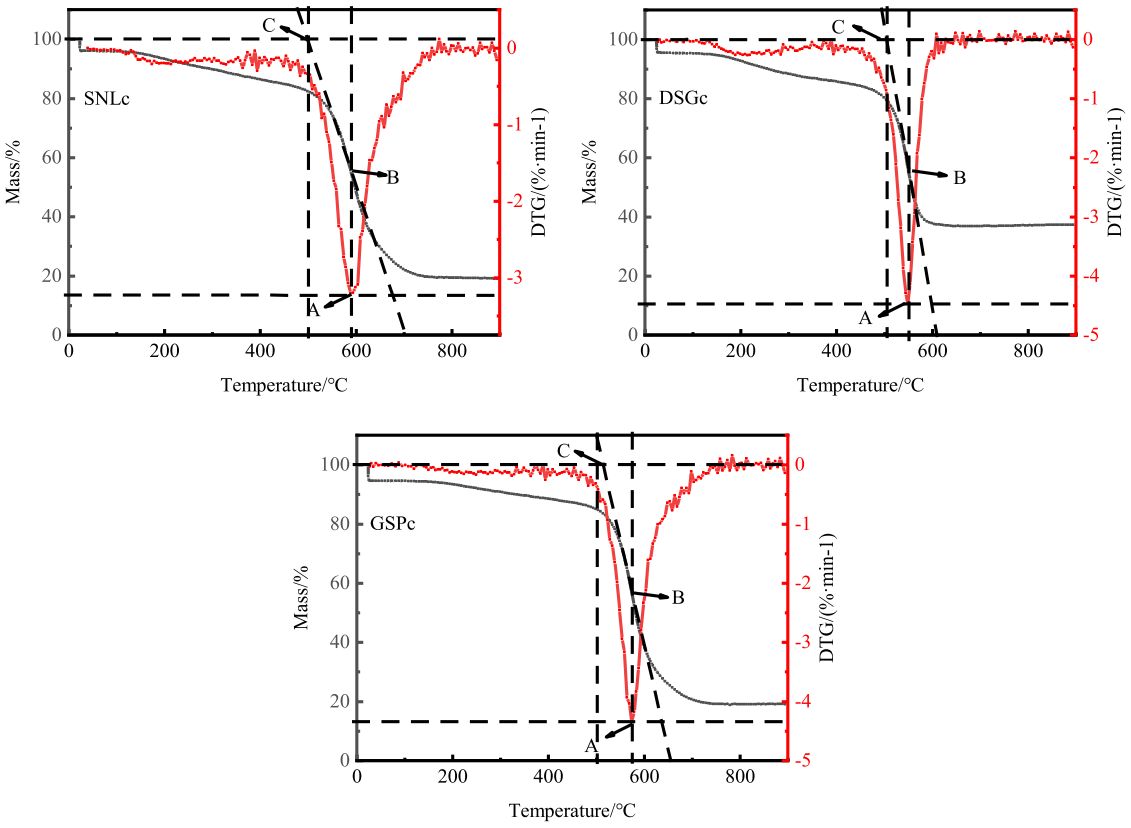

Figure 8. Thermogravimetric analysis of residual carbon products.

Table 10. Characteristic Parameters of the Combustion Curves

item	t_i (°C)	t_h (°C)	t_{peak} (°C)	W_{max} (%·min^{-1})	W_{mean} (%·min^{-1})	S (%^{2}·min^{-2}·°C^{-3})
SNLc	500.14	738.91	588.85	3.20	1.29	2.25×10^{-8}
DSGc	505.67	718.84	573.95	4.34	1.43	3.52×10^{-8}
GSPc	501.16	638.82	549.10	4.47	1.52	4.47×10^{-8}

4. CONCLUSIONS

The above-mentioned results lead us to the following conclusions:

(1) The three kinds of coal gasification fine slag can be separated to different extents in terms of HHS, carbon elements enriched in concentrates, and metal elements and silicon elements enriched in tailings. This can facilitate the low-cost disposal of coal gasification fine slag and the resource recycling of carbon products.

(2) HHS is jointly affected by the pore structure, the surface functional group, the surface element distribution, and the carbon/ash distribution form of coal gasification fine slag. The ash distributed in the residual carbon surface and the matrix space with different particle sizes was removed and that in the carbon−ash melt was difficult to separate. The developed pore structure consumes the agent, and the hydrophilic functional group and hydrophilic material do not favor the adhesion of the agent.

(3) The combustion characteristics of residual carbon in the three types of coal gasification fine slag concentrate were studied by Raman spectrometry and thermogravimetric analysis. This is mainly due to the residual carbon in GSP_C having a large specific surface area and less ash materials, resulting in an accelerated diffusion capacity of the air, more amorphous carbon structures (less graphitic), and more abundant active sites, which strengthen the combustion activity.

AUTHOR INFORMATION

Corresponding Author

Lianping Dong − *College of Mining Engineering, Taiyuan University of Technology, Taiyuan 030024 Shanxi, China;* orcid.org/0000-0002-3096-982X; Email: 120107193@qq.com

Authors

Zhonghua Xue − *College of Mining Engineering, Taiyuan University of Technology, Taiyuan 030024 Shanxi, China;* orcid.org/0000-0002-5997-7719

Xiaoting Fan − *State Key Laboratory of Clean and Efficient Coal Utilization, Taiyuan University of Technology, Taiyuan 030024 Shanxi, China;* orcid.org/0000-0001-8451-8672

Zhenyang Ren − *State Key Laboratory of Clean and Efficient Coal Utilization, Taiyuan University of Technology, Taiyuan 030024 Shanxi, China;* orcid.org/0000-0002-7561-642X

Xiaodong Liu − *State Key Laboratory of Clean and Efficient Coal Utilization, Taiyuan University of Technology, Taiyuan 030024 Shanxi, China;* orcid.org/0000-0002-6013-302X

https://doi.org/10.1021/acsomega.2c00484
ACS Omega 2022, 7, 16484−16493

Panpan Fan − *State Key Laboratory of Clean and Efficient Coal Utilization, Taiyuan University of Technology, Taiyuan 030024 Shanxi, China;* orcid.org/0000-0003-4255-4979
Minqiang Fan − *College of Mining Engineering, Taiyuan University of Technology, Taiyuan 030024 Shanxi, China;* orcid.org/0000-0002-6490-5621
Weiren Bao − *State Key Laboratory of Clean and Efficient Coal Utilization, Taiyuan University of Technology, Taiyuan 030024 Shanxi, China;* orcid.org/0000-0003-3822-0239
Jiancheng Wang − *State Key Laboratory of Clean and Efficient Coal Utilization, Taiyuan University of Technology, Taiyuan 030024 Shanxi, China;* orcid.org/0000-0001-5928-2792

Complete contact information is available at: https://pubs.acs.org/10.1021/acsomega.2c00484

Author Contributions

Z.X.: conceptualization, study experiments, data curation, formal, analysis, investigation, project administration, validation, visualization, and writing—original draft. L.D.: funding acquisition, formal analysis, investigation, methodology, project administration, resources, validation, and writing—review and editing. X.F.: conceptualization, methodology, resources, validation, and writing—review and editing. Z.R.: methodology, resources, validation, and writing—review and editing. X.L.: validation and writing—review and editing. P.F.: funding acquisition, investigation, and resources. M.F.: writing—review and editing. W.B.: investigation and project administration. J.W.: investigation and project administration.

Notes

The authors declare no competing financial interest.

■ ACKNOWLEDGMENTS

Acknowledgment goes to the Taiyuan University of Technology for providing the research facilities. Financial support was provided Chinese national key research and development program-funded projects (2019YFC1904302) which belongs to L.D. and the State Key Laboratory of High-efficiency Utilization of Coal and Green Chemical Engineering, Ningxia University (2021-K81) which belongs to P.F. The authors greatly appreciate the support and assistance of these institution personnel.

■ REFERENCES

(1) Wang, Q.; Song, X. X. Why do China and India burn 60% of the world's coal: A decomposition analysis from a global perspective. *Energy* **2021**, *227*, No. 120389.
(2) Guo, Q. H.; Wei, J. T.; Gong, Y.; Zhu, H. W.; Yu, G. S. Research progress on hot-model behavior of opposed multi-burner entrained-flow gasification. *J. China Coal Soc.* **2020**, *45*, 403−413.
(3) China National Coal Association. *Guidance on Modern Coal Chemical Industry Development in the 14th Five-Year Plan of Coal Industry*. China Coal Resources Network: China; 2021.
(4) Xu, S. Q.; Zhou, Z. J.; Gao, X.; Yu, G. S. The gasification reactivity of unburned carbon present in gasification slag from entrained-flow gasifie. *Fuel Process. Technol.* **2009**, *90*, 1062−1070.
(5) Wu, T.; Gong, M.; Lester, E. Characterisation of residual carbon from entrained-bed coal water slurry gasifiers. *Fuel* **2007**, *86*, 972−982.
(6) Ma, W. P.; Liu, S. Q.; Li, Z. Release and transformation mechanisms of hazardous trace elements in the ash and slag during underground coal gasification. *Fuel* **2020**, *281*, No. 118774.
(7) Wang, Y. F.; Tang, Y. G.; Li, R. Q.; Guo, X.; Hurley, J. P.; Finkelman, R. B. Measurements of the leachability of potentially hazardous trace elements from solid coal gasification wastes in China. *Sci. Total Environ.* **2021**, *759*, No. 143463.
(8) Guo, F. H.; Zhao, X.; Guo, Y.; Zhang, Y. X.; Wu, J. J. Fractal analysis and pore structure of gasification fine slag and its flotation residual carbon. *Colloids Surf., A* **2020**, *585*, No. 124148.
(9) Shi, Z. C.; Dai, G. F.; Wang, X. B.; Dong, Y. S.; Li, P.; Yu, W.; Tan, H. Z. Review on the comprehensive resources utilization technology of coal gasification fine slag. *Huadian Technol.* **2020**, *42*, 63−73.
(10) Li, H. Z.; Dong, L. P.; Bao, W. R.; Wang, J. C.; Fan, P. P.; Fan, M. Q. Carbon-ash Separation of coal gasification slag in swirling water based on apparent density. *Chem. Ind. Eng. Prog.* **2021**, *40*, 1344−1353.
(11) Wu, Y. Study on the Separation and Utilization of Gasified Residues. Dissertation, Xi'an University of Science and Technology: Xi'an, 2017.
(12) Dong, L. P.; Fan, P. P.; Fan, M. Q.; Bao, W. R.; Wang, J. C. A Device and Method for Reselecting Carbon Ash Separation by Gasification Slag Water Interspin Flow. Chinese Patent CN111659527A2020.
(13) Ren, Z. Y.; Jing, Y. H.; Fan, P. P.; Gao, Y. C.; Dong, L. P.; Bao, W. R.; Fan, M. Q.; Chang, L. P. Experimental study on the water-medium gravity separation of gasification slag and the preparation of desulfurization and denitrification activated coke using separated carbon. *J. China Coal Soc.* **2021**, *46*, 1164−1172.
(14) Ge, X. D. Surface properties analysis of coal gasification coal cinder and Hotation extraction research. *China Coal* **2019**, *45*, 107−112.
(15) Wu, S. P.; Zhao, K.; Dong, Y. S.; Wang, X. B.; Bai, Y. H.; Liu, L. J.; Yu, W. Research progress on flotation decarburization of gasified fine slag. *Huadian Technol.* **2020**, *42*, 81−86.
(16) Guo, F. H.; Zhao, X.; Guo, Y.; Zhang, Y. X.; Wu, J. J. Fractal Analysis and Pore Structure of Gasification Fine Slag and Its Flotation Residual Carbon. *Colloids Surf., A* **2019**, *585*, No. 124148.
(17) Hu, J. Y. Study on the Comprehensive Utilization of a Coal Gasification Slag in the North. Dissertation, Southwest University of Science and Technology: Mianyang, 2018.
(18) Wang, X. B.; Fu, J. G.; Zhao, D.; Huang, Y. D. Flotation and quality improvement of gasified fine slag carrier. *Coal Eng.* **2021**, *53*, 155−159.
(19) Zhao, S. Y.; Wu, Y.; Li, B. Study on residue features and decarbonization of Texaco entrained flow gasifier. *Coal Eng.* **2016**, *48*, 29−32.
(20) Wang, W. D.; Liu, D. H.; Tu, Y. Y.; Jin, L. Z.; Wang, H. Enrichment of residual carbon in entrained-flow gasification coal fine slag by ultrasonic flotation. *Fuel* **2020**, *278*, 118−195.
(21) Fan, G. X.; Zhang, M. Y.; Peng, W. J.; Zhou, G. L.; Deng, L. J.; Chang, L. P.; Gao, Y. J.; Li, P. Clean products from coal gasification waste by flotation using waste engine oil as collector: Synergetic cleaner disposal of wastes. *J. Cleaner Prod.* **2020**, *286*, No. 124943.
(22) Guo, F. X.; Mao, Z. K.; Zhen, K.; Li, J.; Zhang, Y. X.; Wu, J. J. Properties of flotation residual carbon from gasification fine slag. *Fuel* **2020**, *267*, No. 117043.
(23) Zhang, Y. X.; Guo, Y.; Wang, R. M.; Jia, W. K.; Guo, F. H.; Wu, J. J. Study on the physicochemical properties of Ningdong coal gasification fine slag and its carbon-ash separation products. *J. China Coal Soc.* **2021**, DOI: 10.13225/j.cnki.jccs.FX21.0892.
(24) Yoon, R. H.; Eraydin, M. K. Cleaning and Dewatering Fine Coal. U.S. Patent US9789492B22018.
(25) Yoon, R. H.; Luttrell, G. H. Method for Dewatering Fine Coal. U.S. Patent US54587861995.
(26) Xue, Z. H.; Dong, L. P.; Liu, A.; Fan, M. Q.; Yang, C. Y.; Wang, J. C.; Bao, W. R.; Fan, P. P. Feasibility and mechanism analysis of hydrophobic-hydrophilic separation on the carbon from coal gasification fine slag. *J. China Coal Soc.* **2021**, https://kns.cnki.net/kcms/detail/11.2190.TD.20211110.1812.009.html.
(27) Qu, J. S.; Zhang, J. B.; Sun, Z. G.; Yang, C. N.; Shi, D.; Li, S. P.; Li, H. Q. Research progress on comprehensive utilization of coal gasification slag. *Clean Coal Technol.* **2020**, *26*, 184−193.
(28) Dong, Y. B. Recovery and recycling of carbon resource from fine dregs of water-coal slurry gasification. *Nitrogenous Fertilizer Technol.* **2018**, *39*, 25−27.

(29) Li, Z. H.; Zhang, Y. Y.; Zhao, H. Y.; Chen, H. X.; He, R. Structure characteristics and composition of hydration products of coal gasification slag mixed cement and lime. *Constr. Build. Mater.* **2019**, *213*, 265−274.
(30) Li, X. J.; Hayashi, J. I.; Li, C. Z. FT-Raman spectroscopic study of the evolution of char structure during the pyrolysis of a Victorian brown coal. *Fuel* **2006**, *85*, 1700−1707.
(31) Han, Y. N.; Liao, J. J.; Bai, Z. Q.; Bai, Z. Q.; Bai, J.; Li, X.; Li, W. Correlation between the combustion behavior of brown coal char and its aromaticity and pore structure. *Energy Fuels* **2016**, *30*, 3419−3427.
(32) Wu, J. Z.; Wang, B. F.; Cheng, F. Q. Thermal and kinetic characteristics of combustion of coal sludge. *J. Therm. Anal. Calorim.* **2017**, *129*, 1899−1909.
(33) Wang, X.; Li, S.; Adeosun, A.; Li, Y.; Vujanovic, M.; Tan, H.; Duic, N. Effect of potassium-doping and oxygen concentration on soot oxidation in O_2/CO_2 atmosphere: A kinetics study by thermogravimetric analysis. *Energy Convers. Manage.* **2017**, *149*, 686−697.
(34) Zhou, J.; Lv, J. F. Study on combustion characteristics of petroleum coke at different heating rates by using thermogravimetry. *Coal Convers.* **2006**, *29*, 39−43.

https://doi.org/10.1021/acsomega.2c00484
ACS Omega 2022, 7, 16484−16493